Molecular dynamics study of the hydration of Lennard-Jones solutes

A. Geiger

Institut für Physikalische Chemie und Elektrochemie der Universität Karlsruhe, West Germany

A. Rahman

Argonne National Laboratory, Argonne, Illinois 60439

F. H. Stillinger

Bell Laboratories, Murray Hill, New Jersey 07974
(Received 8 May 1978)

In order to clarify the nature of hydrophobic interactions in water, we have used the molecular dynamics simulation method to study a system comprising two Lennard-Jones solute particles and 214 water molecules. Although the solutes were placed initially in contact, forces in the system drive them slightly apart to permit formation of vertex-sharing solvent "cages." Definite orientational preferences have been observed for water molecules in the first solvation layer around the Lennard-Jones solutes; these preferences are loosely reminiscent of structure in clathrates. Nevertheless, substantial local disorder is obviously present. The dynamical data show that translational and rotational motions of solvation-sheath water molecules are perceptibly slower (by at least 20%) than those in pure bulk water.

I. INTRODUCTION

Computer simulation studies recently have provided important insights into the molecular structure and dynamics of pure liquid water. One set of such studies has been based upon the "ST2" pair potential for rigid water molecules.[1,2] The extent of success in reproducing measured properties of real water by means of this potential model in simulations suggests that it would be useful to treat aqueous solutions along similar lines. This paper reports one such extension.

From the standpoint of molecular dynamics calculations with the ST2 potential the simplest aqueous solution to study would be that which involves nonpolar Lennard-Jones solutes. This observation rests on the facts (a) that no new interactions need to be introduced beyond those already present in the pure-water ST2 model and (b) that only minor changes are required in the water simulation computer program.[3]

It should be noted in passing that Dashevsky and Sarkisov[4] have reported a Monte Carlo simulation of spherical nonpolar solutes in water. Rather different interaction potentials were used in that study leading to uncertainty in how one might rationally compare their results with those reported here.

Solutes that either are nonpolar or which contain bulky nonpolar groups, display an intriguing richness of solution behavior in the solvent water. This collection of unusual phenomena (and their tentative explanations in molecular terms) is usually summarized under the terms "hydrophobic hydration" and "hydrophobic interaction."[5-8] Continuing scientific interest in these matters naturally has been encouraged by the realization that they are directly relevant to fundamental biochemical processes.

Over the years, several structural models for hydrophobic effects have evolved in the light of available thermodynamic and spectroscopic data. These and other aspects of the subject are comprehensively reviewed in the *Water* series edited by Franks.[6]

The low solubility of nonpolar molecules in water (due primarily to negative entropy of hydration) as well as marked solution heat-capacity effects produced by those molecules, led Frank and Evans to postulate their "iceberg model" of hydration.[9] Enhanced "icelikeness" of the water near the inert particles was supported by statistical-thermodynamic analysis of Nemethy and Scheraga.[10] Kauzmann has reviewed the role played by nonpolar-group interactions in biopolymers. The "hydrophobic bond" or the association of nonpolar groups or molecules can be regarded as a partial reversal of the thermodynamically unfavorable process of solution. Kauzmann has also cautioned that the phrase "iceberg formation" should not be taken literally when describing structure promotion in the hydration shell. Hertz has proposed using molecular pair correlation functions to describe the structure-changing influence of solutes in a quantitative way.[7,11] Glew postulated a clathratelike water environment for nonpolar molecules, acknowledging the existence and stability of solid gas hydrates[12]; he also noted that the solvating water molecules in the liquid solutions are doubtless subject to far less stringent orientational constraints than those present in solid clathrates.

Experimental findings sometimes are ambiguous. For example, proton chemical shift measurements at room temperature indicate a weakening of hydrogen bonds near nonpolar solutes,[13] whereas downfield shifts at 0 °C indicate structure promotion.[14,15] Nuclear magnetic relaxation studies show slowing of molecular motion in the vicinity of the nonpolar solute,[16,17] although to such a small extent that no rigid hydration cage can be assumed. This slowing is also supported by dielectric relaxation measurements.[18] Nuclear magnetic relaxation results provide additional information about orientation of hydration-shell water, and they can be

 0021-9606/79/010263-14$01.00

explained by clathratelike preferences.[19,20]

Experimental findings are indeed diverse and suggestive, but at the same time no uniquely supported molecular picture has emerged. Perhaps one could at least conclude that the appearance of hydrophobic hydration is not terribly sensitive to details of the water–solute pair potential (if the latter is nonpolar). Thus it is in this setting that we proposed to use molecular dynamics with simple Lennard-Jones solutes, to generate a more detailed and vivid molecular view of hydrophobic hydration.

II. MOLECULAR DYNAMICS OUTLINE

In a previous study of the solvation behavior of ST2 water[3] a preliminary simulation run for the present system was generated. We have continued to use the general procedure of that study. Starting with a pure water configuration of 216 molecules in equilibrium, two immediate neighbors are chosen and changed to Lennard-Jones particles. This change is accomplished as follows: When calculating the Cartesian coordinates of the oxygen and the four point charges of the ST2 model via the center of mass coordinates, the Euler angles, and the internal coordinates of the five positions in the molecule, these two particles are treated as if all internal coordinates of the two are zero; also the four partial charges are set to zero. All other parameters remain the same. Thus we get a system of two Lennard-Jones spheres with the same mass and the same Lennard-Jones parameters σ and ϵ as the surrounding 214 ST2 water molecules.

Since the Lennard-Jones parameters σ and ϵ were originally chosen (in the BNS potential[1]) to correspond to neon[1] we call these particles "neons" for brevity, although (in the ST2 potential) σ and ϵ were later modified,[2] so that when using σ, ϵ of the ST2 potential we actually have two Lennard-Jones particles somewhere in between neon and argon. The water–water interaction potential $V_{WW}(\mathbf{x}_i, \mathbf{x}_j)$ is as described earlier[2]

$$V_{WW}(\mathbf{x}_i, \mathbf{x}_j) = V_{LJ}(r_{ij}) + S(r_{ij}) V_{el}(\mathbf{x}_i, \mathbf{x}_j) \ .$$

The Lennard-Jones part V_{LJ} acts between the oxygens, $V_{el}(\mathbf{x}_i, \mathbf{x}_j)$ describes the Coulomb interaction for the 16 pairs of point charges and is modulated by the switching function $S(r_{ij})$, which is given by

$$\begin{aligned} S(r_{ij}) &= 0 && (0 \le r_{ij} \le R_L) \ , \\ &= \frac{(r_{ij} - R_L)^2 (3R_u - R_L - 2r_{ij})}{(R_u - R_L)^3} , && (R_L \le r_{ij} \le R_u) \ , \\ &= 1 && (R_u \le r_{ij}) \ . \end{aligned}$$

The water–neon and neon–neon potentials are

$$V_{NeW}(r) = V_{NeNe}(r) = V_{LJ}(r) = 4\epsilon[(\sigma/r)^{12} - (\sigma/r)^6] \ ,$$

r is the Lennard-Jones center distance, $\sigma = 3.1$ Å, $\epsilon = 5.2605 \times 10^{-15}$ erg $= 75.75$ cal/mole. The mass density of 1 g/cm^3 and consequently the cube edge length of the periodicity box of 18.62 Å was the same as in the pure water studies.

The total energy of the 216 particles was specified to be -105.7ϵ per particle. A cutoff distance $R_c = 7.05$ Å was chosen, beyond which interactions were disregarded. This seemingly small value was chosen for several reasons. From a previous test run it was concluded that relatively slowly varying structural fluctuations were present, so that a very long run was expected to be necessary; consequently a small R_c would save computer time. On the other hand the main interest was directed to microstructural and microdynamic properties in the immediate vicinity of the solute, which are probably less affected by this choice than are the thermodynamic properties. Also, mainly differences between bulk and shell water were investigated, so that for several properties contributions from more distant interacting partners can be expected to cancel out in large measure.

The time step τ for the numerical integration of the dynamical equations was $\tau = 2.1261 \times 10^{-16}$ sec as in the pure water calculations.

Due to the cutoff and numerical "noise" the total energy is not strictly conserved. For this reason, this property was monitored every 10 times steps and if it had shifted by more than $\pm 0.05\epsilon$ (occurring on the average every 80τ), all momenta were rescaled to recover the initial energy value.

The temperature of the system, calculated from the average total kinetic energy, was $32.3\,^\circ\text{C} = 305.5\,^\circ\text{K}$.

III. NEON PAIR MOTION

After creation of the system from pure water as described before, an "equilibration" calculation of about 8000 time steps was carried out; the first 1600 steps of these were taken with increased moments of inertia and increased time step size.[21] Then about 25 000 time steps followed that were used for analysis. Figure 1(a) shows the neon–neon distance d as a function of time during this analysis period and after the equilibration part of the run had been discarded.

During the first 2.5 psec the two neons are trapped together in a cavity without any water between them, so that they can approach each other to about 2.8 Å. Then they separate and a new "two cage" configuration builds up, where one water layer is situated between the two neons. During this latter period they cannot come closer than approximately 5.0 Å, while having a mean distance of about 6.0 Å.

Figure 1(b) shows the configuration of the water molecules in the layer between the two neons at moments of closest approach, indicated by arrows in Fig. 1(a). For these diagrams a special coordinate system ξ, η, ζ is used. The ζ-axis points along the line joining the two neons, with the origin at the midpoint. The ξ, η positions of all water molecules which are members of the intermediate layer (defined by the two neon positions along the ζ axis), and which have a distance of less than 4.2 Å from at least one neon are identified. The Lennard-Jones spheres of the molecules are indicated by circles of radius $r = 1.4$ Å $= 0.45\,\sigma$. (Also the molecule number is indicated). In the center of the ξ, η-coordinate system, the overlapping circles due to the neons are shown as shaded circles; in other words the diagrams show the configuration as seen by looking down

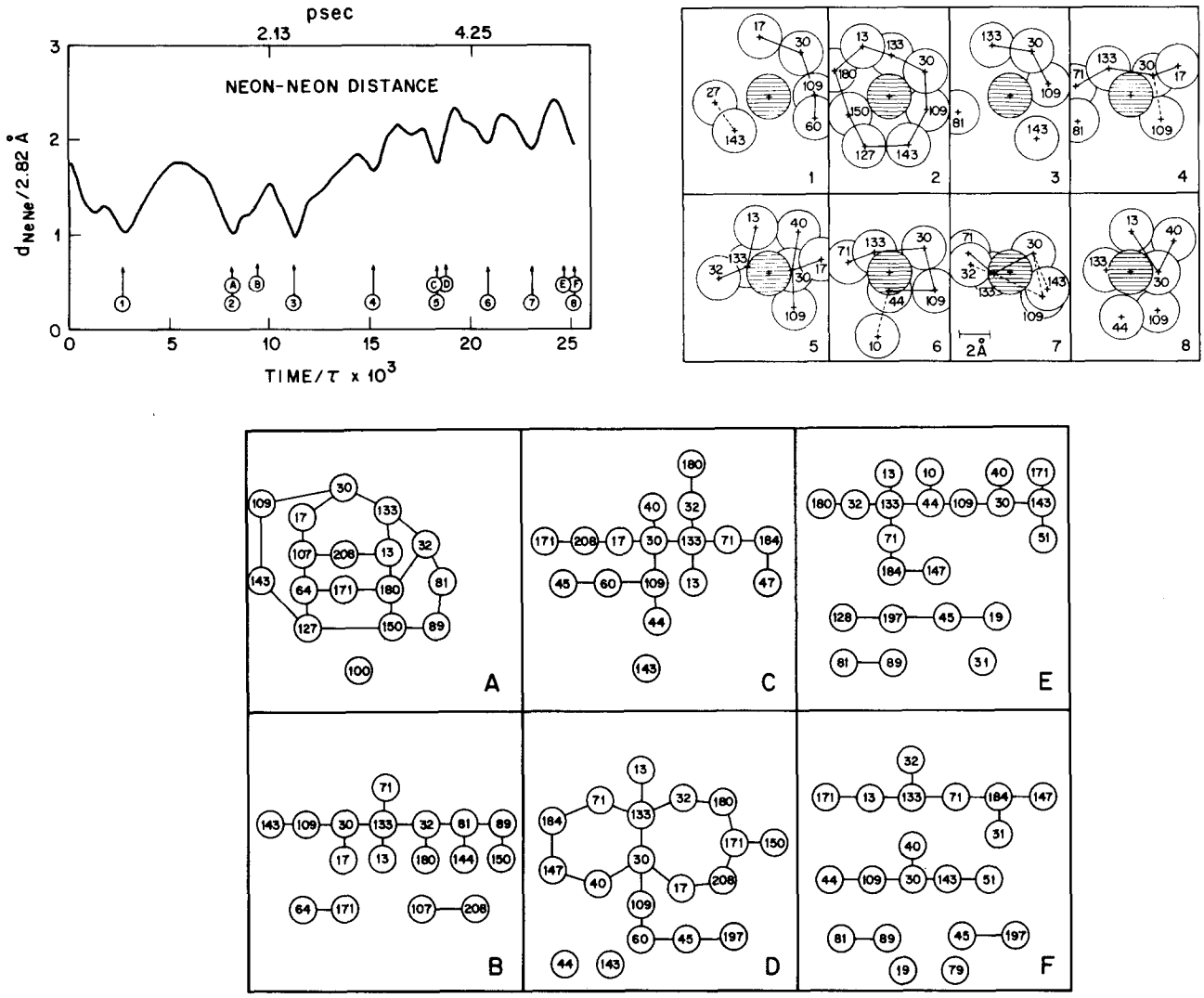

FIG. 1. (a) Neon–neon distance d as a function of time during the analysis period; $d(t) = |\mathbf{r}_{Ne1}(t) - \mathbf{r}_{Ne2}(t)|$. Arrows refer to diagrams of Fig. 1(b) and (c). Time is given in units of 10^{-12} sec and of simulation run time step τ. d is given in units of 2.82 Å. (b) Configuration of the water molecules in the layer between the two neons as seen by looking down the neon–neon axis at moments indicated by arrows in Fig. 1(a). The overlapping neons are shown as shaded circles. Pair interaction energies $V_{ij} < -40\epsilon$ are indicated by full lines. Broken lines correspond to $-40\,\epsilon \leq V_{ij} \leq -20\,\epsilon$; $\epsilon = 75.75$ cal/mole. (c) Hydrogen bond patterns formed among the water molecules with a center-of-mass distance less than 4.2 Å to at least one neon; pairs with interaction energies $V_{ij} < -40\,\epsilon$ are connected by lines.

the ζ axis. In Fig. 1(b), strong attractive pair interactions between molecules are indicated by full lines when $V_{ij} \leq -40\epsilon$ and by broken lines for $-40\epsilon < V_{ij} \leq -20\epsilon$.

No rigid geometrical arrangement, comparable to a hydrate structure or ice crystal lattice can be recognized. Nevertheless it is quite remarkable that one tight bond (between molecules #30 and #133) persists for a rather long time and is situated between the neon pair; such a behavior was also observed in the preceding study.[3] It is likely (and the structural analysis in the next section will confirm it) that this pair (molecules #30 and #133) forms a common edge of the two adjacent hydration cages. Very recently it was stated[22] that the existence of such a configuration could involve a reduction in the free energy, leading to a stabilization of a solvent-separated hydrophobic association.[7]

Although a quantitative analysis of water pair interaction will follow in Sec. V, it is interesting to discuss in this present connection some hydrogen bond patterns [Fig. 1(c)]. All water molecules with a center of mass distance d_s of less than 4.2 Å to at least one neon are collected and in this collection all pairs with interaction energies $V_{ij} \leq -40\epsilon$ are connected by lines. (By hindsight it seems that d_s was chosen too small, because the first hydration shell extends up to 4.8 Å as we shall see later, so that it is probable that further bond "bridges" within the first hydration shell are not monitored.) The diagrams A, B....F correspond to the times shown by the same symbols in Fig. 1(a). Two diagrams are striking. Diagram A shows a highly connected single water cage, enclosing both neons, whereas in diagram D two adjacent closed rings, connected by the earlier identified water pair (#30 and #133) can be recognized,

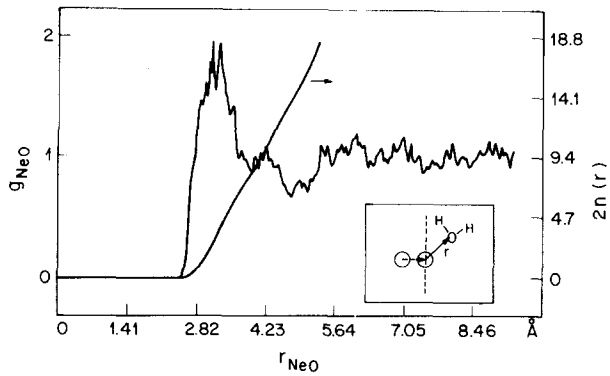

FIG. 2. Neon–oxygen pair correlation function $g_{NeO}(r)$ for the "undisturbed" part of the water environment of the neon pair (see insert). Values of $2n(r)$ indicated on the right-hand scale give the running coordination number of a complete hydration shell, composed of two undisturbed halves.

supporting the connected cage picture.

It must be stressed that the considerations of this section lack compelling statistical significance, and thus can only be regarded as hints as to how hydrophobic interaction may occur. In the following sections our emphasis will be devoted to the question of hydrophobic hydration only.

IV. STRUCTURE OF THE HYDRATION SHELL

A. Neon-oxygen radial pair correlation function

Description of the neon hydration shell structure can be initiated with the neon–oxygen radial pair correlation function $g_{NeO}(r)$. To stress relevant features, this function is calculated only for those neon–water pairs for which

$$\mathbf{r}_{c\alpha} \cdot \mathbf{d}_{\alpha\beta} \geq 0 ,$$

$$\mathbf{r}_{c\alpha} = \mathbf{r}_{cw} - \mathbf{r}_{Ne\alpha} ,$$

$$\mathbf{d}_{\alpha\beta} = \mathbf{r}_{Ne\alpha} - \mathbf{r}_{Ne\beta} .$$

$\mathbf{r}_{Ne\alpha}$, $\mathbf{r}_{Ne\beta}$ are the position vectors of the two neons and $\mathbf{r}_{cw}$ the position vector of the center of mass of the water molecule.

With this restriction $g_{NeO}(r)$ is not unduly obscured by the presence of the second neon and describes the undisturbed part of the hydration shell (Fig. 2). The figure also shows the "running coordination number" which is given by

$$n_{NeO}(r) = 2\pi\rho_0 \int_0^r s^2 g_{NeO}(s) ds .$$

The factor 2π appears because we have only a half-shell as specified above. We deduce from this that the number of nearest neighbors in the complete hydration shell of a *single* neon at infinite dilution will be given approximately by $2 \times n_{NeO}(r)$. Thus Fig. 2 suggests that there are $2n_{NeO}(4.8\ \text{Å}) = 14$ nearest neighbors in a hydration shell around a neon at infinite dilution. This coordination is similar to that found in pure L-J systems.[23] To carry the inference even further, we note the distinct shoulder between 3.9 and 4.8 Å (see Fig. 2) suggesting a subdivision of the entire hydration shell into two subshells containing 8 and 6 molecules, respectively. As will be seen later these subshells (around the two neons we have in the present calculation) show different preferential orientations of the water molecules which can be explained by a clathratelike hydration structure.

B. Orientational structure of the undisturbed hydration shell

Orientational distribution functions were calculated separately for two geometrically defined shells, surrounding the neon atoms, roughly equivalent to the just-mentioned two subshells. To avoid ambiguities due to the mixing of differing structures developing in time, analysis was effected separately for two different time periods. Period I. Between $t_1 = 0$ and $t_2 = 12\,000\tau = 2.55$ psec, when the neons are close together and enclosed in one water cage. Period II. Between $t_3 = 15\,000\tau = 3.19$ psec and $t_4 = 25\,360\tau = 5.39$ psec, when the neons are separated by a water monolayer and occupy two different but adjacent water cages [see Fig. 1(a)].

Figure 3 shows the distribution of orientations of the water OH bonds with respect to the neon–oxygen vector in the first subshell of the undisturbed hydration shell during time period II.

$$\cos\alpha = \hat{\mu}_{OH} \cdot \hat{\mu}_{ONe} ,$$

$$\hat{\mu}_{OH} = (\mathbf{r}_O - \mathbf{r}_H)/|\mathbf{r}_O - \mathbf{r}_H| ,$$

$$\hat{\mu}_{ONe} = (\mathbf{r}_O - \mathbf{r}_{Ne})/|\mathbf{r}_O - \mathbf{r}_{Ne}| ,$$

for all water molecules with

$$(\mathbf{r}_{Ne\alpha} - \mathbf{r}_{Ne\beta}) \cdot (\mathbf{r}_{cw} - \mathbf{r}_{Ne\alpha}) \geq 0$$

and

$$|\mathbf{r}_{cw} - \mathbf{r}_{Ne\alpha}| \leq 3.7\ \text{Å} .$$

Figure 4 shows the distribution for those water molecules that are members of the second subshell:

$$3.7\ \text{Å} < |\mathbf{r}_{cw} - \mathbf{r}_{Ne\alpha}| \leq 4.5\ \text{Å} .$$

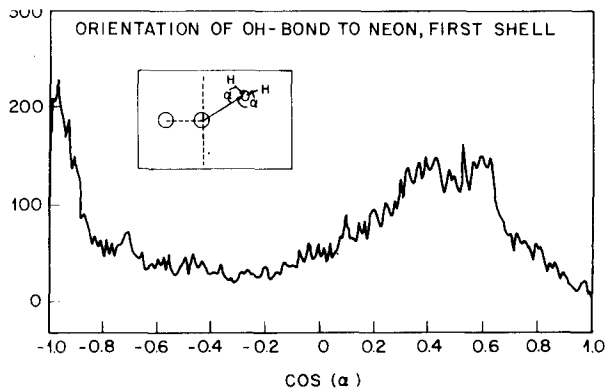

FIG. 3. Distribution function for the angle cosines describing the orientation of the water OH bonds with respect to the neon–oxygen vector (see insert) in the first subshell (neon–water center-of-mass distance $d \leq 3.7$ Å). The distribution is for the undisturbed part of the hydration shell (see insert) during time period II ($t = 15\,000\tau$ to $25\,360\tau$).

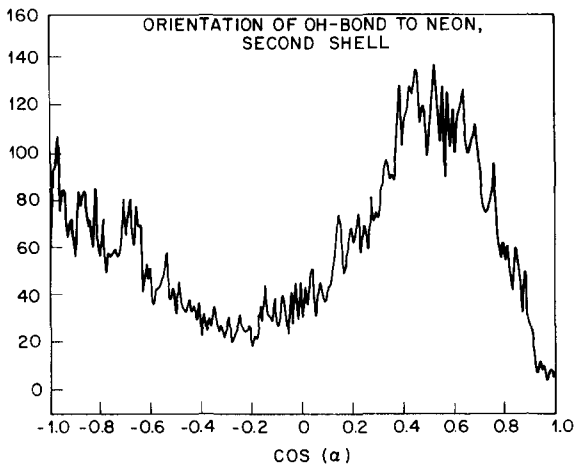

FIG. 4. OH-bond orientation distribution function for the water molecules of the second subshell, $3.7\ \text{Å} < d \leq 4.5\ \text{Å}$ (same restrictions as in Fig. 3).

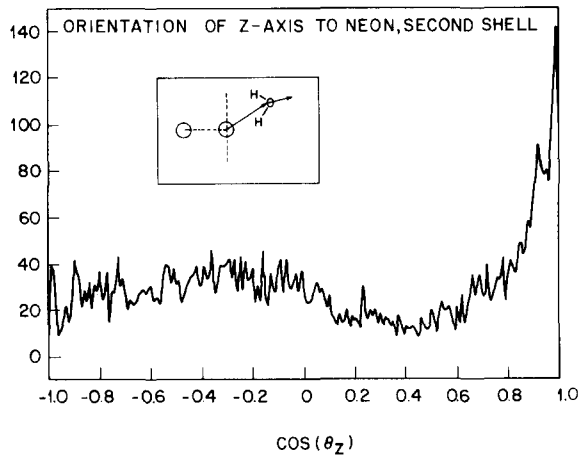

FIG. 6. z-axis orientation distribution function for the water molecules of the second subshell, $3.7\ \text{Å} < d \leq 4.5\ \text{Å}$ (same restrictions as in Fig. 3).

To get some more information about the orientational structure of the hydration sphere, equivalent orientational distribution functions were calculated for the dipole directions of the hydration water molecules. The same coordinate system as in Ref. 1 was used, so that the z axis of the molecule points in the direction opposite to the molecular electric dipole moment.

The z-axis orientation distributions show very pronounced features. Figures 5 and 6 present results for the two subshells (still for time period II and for the undisturbed part of the hydration shell only):

$$\cos\theta_z = \hat{\mu}_{cNe} \cdot \hat{\mu}_z \ ,$$

$\hat{\mu}_z$ is the unit vector in z direction,

$$\hat{\mu}_{cNe} = (\mathbf{r}_{cw} - \mathbf{r}_{Ne}) / |\mathbf{r}_{cw} - \mathbf{r}_{Ne}| \ .$$

The distributions can be interpreted with a geometrical arrangement comparable to Fig. 9 of Ref. 24. From Fig. 3 we infer that the water molecules in the first subshell are oriented in such a way that one of the four tetrahedral bond directions points radially outward, i.e., away from the center of the neon. For each of these eight molecules then the remaining three bond directions straddle the neons ("type 1" molecules[24]). As seen in Fig. 6, in the second hydration subshell however there exists a preferred orientation such that the z axis is oriented radially outward ("type 2" orientation).[24]

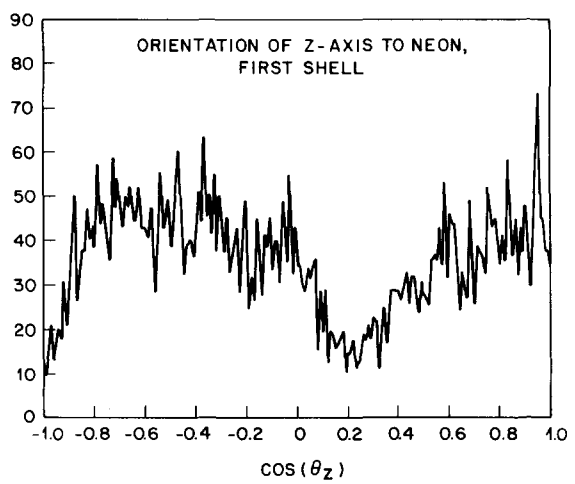

FIG. 5. Distribution function for the angle cosines describing the orientation of the water–molecule z axis with respect to the neon–oxygen vector in the first subshell, $d \leq 3.7$ Å (same restrictions as in Fig. 3).

If one had ideal "type 1" orientation of the water tetrahedron with statistically random distribution of the tetrahedral directions, one would get an OH-bond distribution with one peak at $\cos\alpha = 1.0$, containing one-fourth of all OH bonds and one peak at $\cos\alpha = 0.33$, containing three-fourth of the OH bonds.

In contrast to this ideal situation, we observe (Fig. 3) an orientational distribution with a maximum shifted away from -1.0 corresponding to a tilt of the tetrahedron of about 12°; about half of all water molecules contribute simultaneously to the maxima at $\cos\alpha = 0.97$ and $\cos\alpha \approx +0.5$. The other molecules in the first shell then have OH bonds oriented in such a way that both are straddling the neon, so both contribute to the broad maximum near $\cos\alpha \approx +0.5$. These preferential orientations are reflected in the z-axis orientation distribution (Fig. 5), although less pronounced; in other words they are orientations where both protons point outward symmetrically, so that $\cos\theta_z = -1.0$, and those with one proton pointing radially inward [$\cos\theta_z = \cos(\theta_t/2) \equiv +1/3$, where θ_t is the tetrahedral angle] are avoided.

These results can be compared with conclusions drawn from nuclear magnetic relaxation studies. Hertz *et al.* investigated the orientation of nearest neighbor water molecules surrounding the nonpolar part of methanol and propionic acid[19] and the tetraethylammonium ion.[20] Two different orientations were proposed that could not be distinguished by the NMR method. The first one is equivalent to our slightly tilted radial orientation of one OH bond with tilting angles of up to 6°. The second one resembles those type 1 configurations where both OH bonds approximately parallel the inert particle surface; but the NMR results suggest θ_z to be larger, i.e., the protons point away from the inert group to a larger extent than they do in our simulation. But the

NMR investigations also show that θ_z decreases appreciably with decreasing size of the inert group (from 100° to 81° when proceeding from the tetraethylammonium ion to the methyl group of methanol). Thus the straddling orientation with respect to the Lennard-Jones particle is consistent with the experimentally observed tendency.

In the second hydration subshell the radial OH-bond orientations ($\cos\alpha = -1.0$) are much less abundant and the broad peak at $\cos\alpha \approx +0.5$ is increased (Fig. 4). The z-axis orientation distribution (Fig. 6) shows a strong preference for orientations with the z axis pointing radially outward ($\cos\theta_z = +1.0$). This indicates a tendency towards type 2 orientation in this subshell.

The structure around nonpolar solutes as proposed in Ref. 12 and the structure discussed above for the two-neon case (during time period II) are not contradictory. In fact, the undisturbed hydration shell treated so far can schematically be described by a highly strained net of six hexagonal rings with clathratelike characters. Figure 7(a) shows a perspective drawing of such a structure and Fig. 7(b) a projection along the axis of highest symmetry. As one can see, this net consists of eight type 1 water molecules (full circles) constituting the first subshell, and six type 2 molecules (open circles) of the second hydration subshell further out. These pictures have been given to illustrate the preferential orientations in the hydration shell; they are meant to indicate schematically the possible preferred orientation and bondings that might be present. We note that at any instant only fragments of this structure may be present and that, as we shall see later, hydrogen bonding behavior and mobility of the hydration water are changed only slightly compared to pure water and do not support strongly bonded, rigid clathrate models.

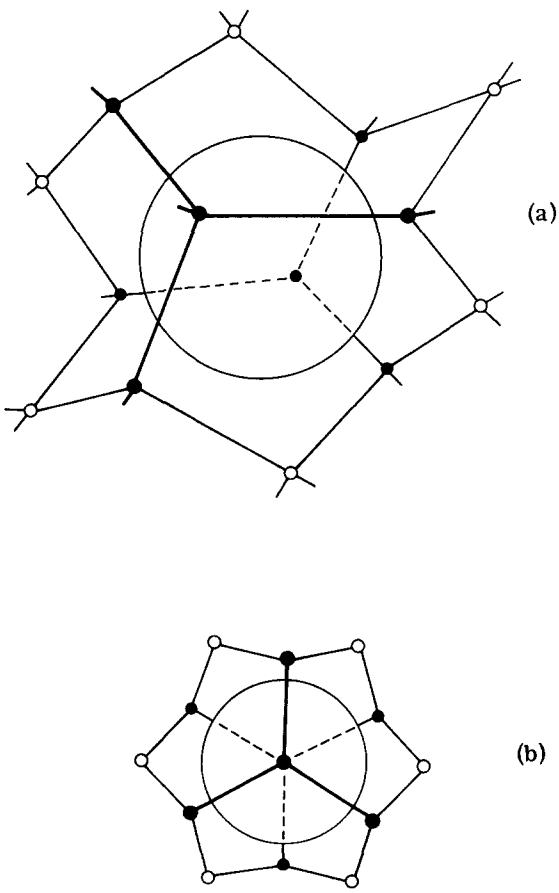

FIG. 7. Example of a hypothetical water-molecule cage enclosing a single LJ solute which would cause distribution functions similar to those obtained in Figs. 2–6. The oxygen nuclei are drawn as circles, possible hydrogen bonds as lines. Filled circles indicate members of the first subshell which are closer to the solute and show a preferred "straddling" orientation. Open circles mark second subshell members, which show preferred radial z-axis orientation. (a) perspective drawing, (b) projection along the axis of highest symmetry.

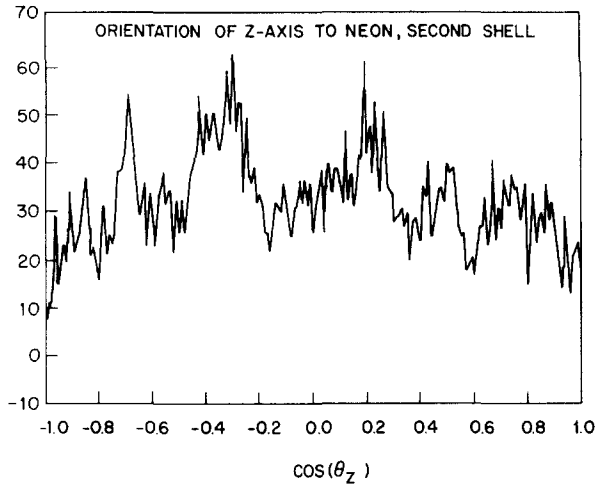

FIG. 8. z-axis orientation distribution function obtained under the same specifications as in Fig. 6, except for the averaging period which is now time period I ($t = 0$–$12\,000\tau$).

During time period I the OH-bond orientation for the same (undisturbed) part of the hydration shell shows a behavior comparable to that during time period II, the distributions being only slightly broader. There is only one striking difference. Type 2 orientations are not preferred in the second subshell during time period I (Fig. 8), as they are in time period II (see Fig. 6).

A possible explanation for this difference is the presence of the second neon. Obviously the cage that surrounds both neons simultaneously during time period I is too large to favor a structure as described for period II. The period II structure becomes possible only when both neons occupy different and hence smaller cages.

C. Orientational structure of the intermediate water

The conclusions given above are based on single- or double-cage pictures; these conclusions are supported by the orientation of those hydration water molecules that were not considered in the preceding and which are located between the two planes perpendicular to the neon–neon axis and containing the center of the Lennard-Jones particles (see insert Fig. 11).

Figures 9 and 10 show the pair correlation function between the center of mass of the neon pair and the center of mass of the surrounding water molecules $g_{ccw}(r)$

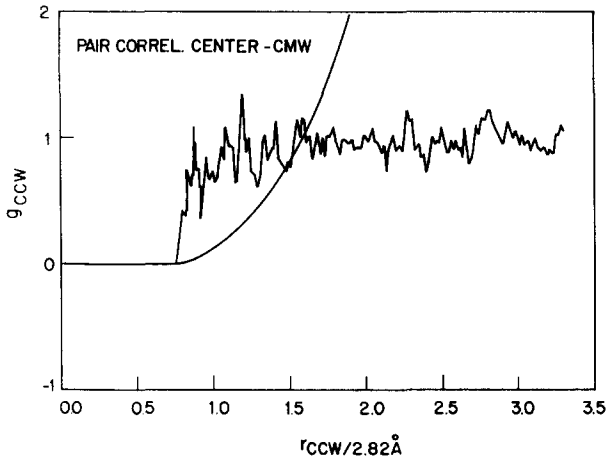

FIG. 9. Pair correlation function $g_{ccw}(r)$ between the center-of-mass of the neon pair and the center-of-mass of the surrounding water molecules, restricted to the "intermediate water layer" (see insert Fig. 11). The averaging is over time period I ($t = 0-12\,000\tau$).

for the two different time periods. During time period I (Fig. 9) the water molecules do not approach the center of mass of the neon pair much closer than they approach the center of the single neons. In contrast during time period II the water molecules show an increased residence probability near the center of mass of the neon pair.

The orientational structure in the intermediate region can be monitored by calculating the distribution of OH-bond orientations with respect to $\mathbf{r}_{Oc}$

$$\mathbf{r}_{Oc} = \mathbf{r}_O - \mathbf{r}_c \,,$$

$$\mathbf{r}_c = (1/2)(\mathbf{r}_{Ne\alpha} + \mathbf{r}_{Ne\beta}) \,.$$

$\mathbf{r}_{Ne\alpha}$, $\mathbf{r}_{Ne\beta}$, $\mathbf{r}_O$ are the position vectors of the two neons and the oxygen nucleus of the water molecule, respectively.

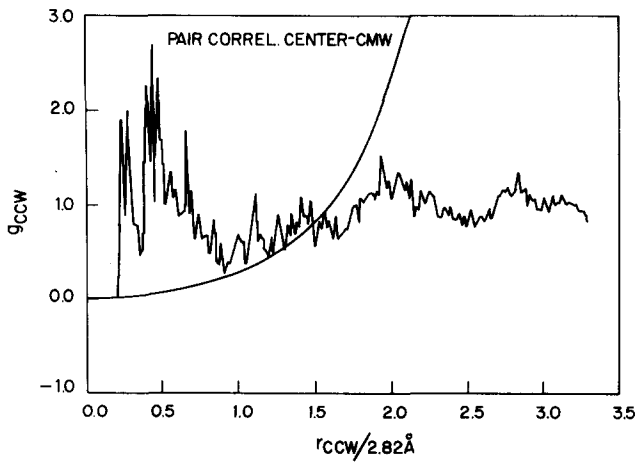

FIG. 10. Same pair correlation function $g_{ccw}(r)$ as in Fig. 9, averaged over time period II ($t = 15\,000$ to $25\,360\tau$). The total absence of events in the small region near $r = 0$ is probably due to insufficient statistics resulting from the finite length of the simulation run. This area should eventually be occupied by some water molecules (in contrast to Fig. 9).

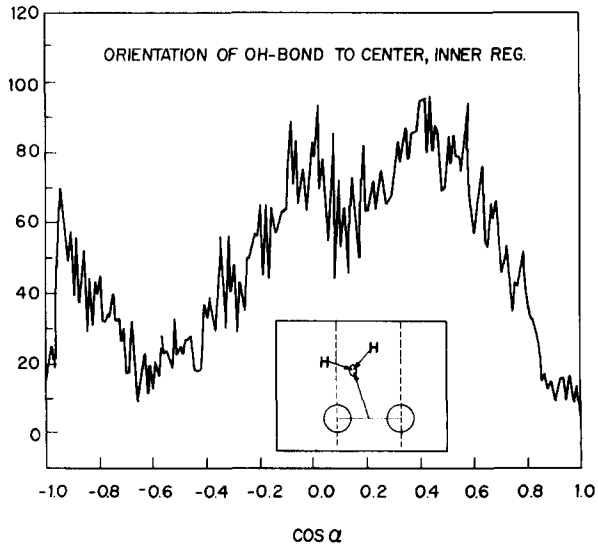

FIG. 11. Distribution function for the angle cosines describing the orientation of the water OH bonds with respect to the vector connecting oxygen to the neon-pair center-of-mass (see insert). Contributions are restricted to water molecules located in the intermediate water layer and having a center-of-mass distance $d_{ccw} = |\mathbf{r}_{cw} - \mathbf{r}_c| \leq 3.7$ Å from the neon-pair center-of-mass. The averaging is over time period I ($t = 0$ to $12\,000\tau$).

$$\cos\alpha = \hat{\mu}_{OH} \cdot \hat{\mu}_{Oc} \,,$$

$$\hat{\mu}_{Oc} = \mathbf{r}_{Oc}/|\mathbf{r}_{Oc}| \,,$$

and $\hat{\mu}_{OH}$ is defined as before. The distribution of the values of $\cos\alpha$ (Figs. 11 and 12) for those water molecules with a distance $d_{ccw} = |\mathbf{r}_{cw} - \mathbf{r}_c| \leq 3.7$ Å from the center of mass of the neon pair and located between the two planes shows a complementary behavior during the two different time periods. The distribution for time period I (Fig. 11) resembles that found in the undisturbed hydration shell and indicates that the water molecules avoid orientations for which one of the four legs of the water tetrahedron points to the center of mass of the neon pair. By contrast during period II this previously avoided orientation is now preferred (see Fig. 12). In adopting these latter orientations it is possible for the

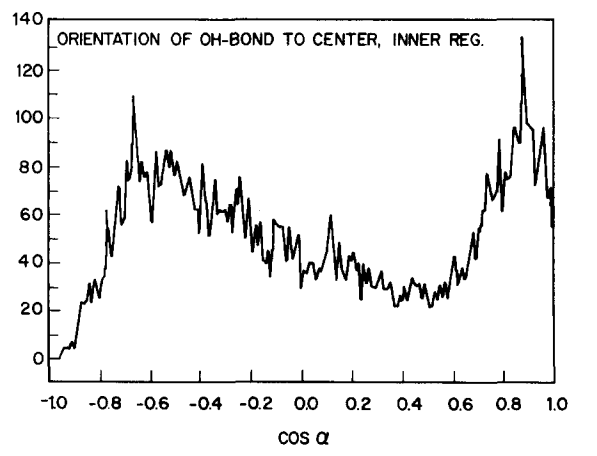

FIG. 12. Same OH-bond orientation distribution function as in Fig. 11, but averaged over time period II ($t = 15\,000\tau$ to $25\,360\tau$).

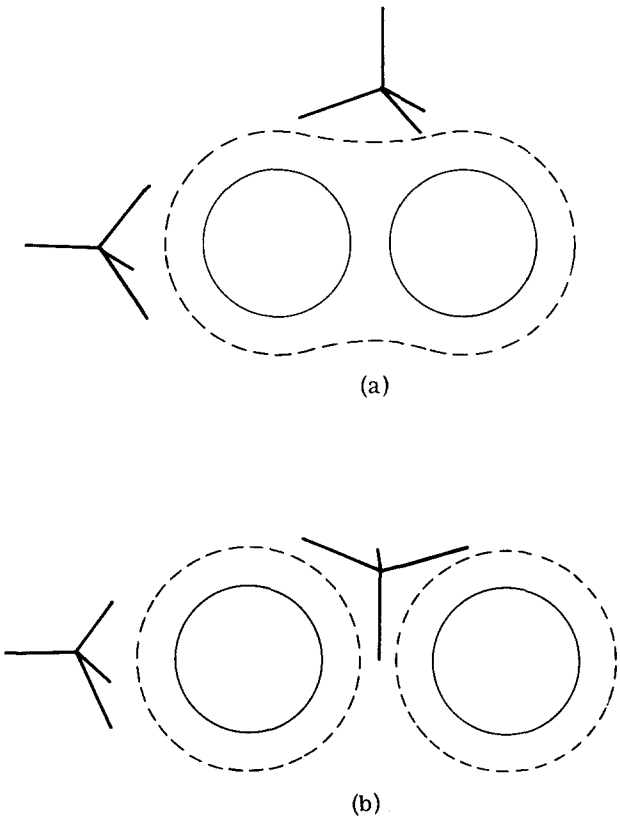

FIG. 13. Schematic characterization of the orientation of the water molecules which constitute the "internal surfaces." (a) One water cage enclosing both neons simultaneously during time period I, (b) two connected cavities containing one neon each during time period II.

members of the intermediate water layer to straddle both neons simultaneously. Figure 13 shows a schematic characterization of this situation.

The above description of the orientation of molecules in the neighborhood of the L-J solute particles can be summarized as follows: All distributions show that those orientations are improbable where one of the tetrahedral bond directions of the water model is perpendicular to the surface of the cavity and pointing inwards, and all those orientations are preferred which allow the four bond directions to be engaged simultaneously in interactions with neighboring water molecules.

D. Water-water radial pair correlation functions

In calculating the intermolecular atom–atom pair correlation functions a distinction has been made between bulk and shell properties. The hydration shell is defined geometrically as before

$$d_{\mathrm{Ne-cw}} = |\mathbf{r}_{\mathrm{Ne}} - \mathbf{r}_{\mathrm{cw}}| \leq 4.5 \text{ Å},$$

and the radial pair correlation about a molecule belonging to the hydration shell is denoted by $g(r)_{\mathrm{shell}}$; hence $g(r)_{\mathrm{bulk}}$ obviously denotes the correlation function about a molecule not belonging to the shell. If in a pair of molecules one member of the pair belongs to the shell and one to the bulk then the atomic distances arising from such a pair contribute to both the $g(r)$'s mentioned above.

TABLE I. Ratios of the heights of the first maximum and the following minimum ($g_{\mathrm{max}}/g_{\mathrm{min}}$) for various water–water pair correlation functions in bulk and shell, and the enhancement factor in proceeding from bulk to shell.

		g_{max}	g_{min}	$g_{\mathrm{max}}/g_{\mathrm{min}}$	Shell/bulk enhancement
g_{OO}	Shell	2.96	0.52	5.69	1.35
	Bulk	3.03	0.72	4.21	
g_{OH}	Shell	1.33	0.25	5.32	1.57
	Bulk	1.25	0.37	3.38	
g_{HH}	Shell	1.40	0.62	2.26	1.30
	Bulk	1.42	0.82	1.73	

Figure 14 shows the two $g_{\mathrm{OH}}(r)$'s. (The O–O and H–H functions have not been displayed.) The quantitative details of all these correlation functions show that (1) The shell functions have 'more' structure than the bulk functions. As a measure of the degree of structure one can take the ratio of the heights of the first maximum and the following minimum. In Table I this ratio is compared and the right-most column gives the enhancement factor in going from bulk to shell. The observed increase in the maxima of these so-called 1–1 distribution functions (i.e., solvent–solvent distributions) was discussed by Hertz[11,7] in an attempt to specify in a precise way the term 'structure making,' when describing the influence of nonpolar solutes in water. (2) It is also interesting to recognize that the position of the first peak of $g_{\mathrm{OH}}(r)$ is not changed discernibly, to be more specific no shift to lower values can be observed in the shell. It is known that NMR experiments show an unexpected up-field shift of the proton resonance at room temperature[13]; this was considered to be contradictory to the otherwise observed structure promotion (although at lower temperature down-field shifts could be measured).[14,15]

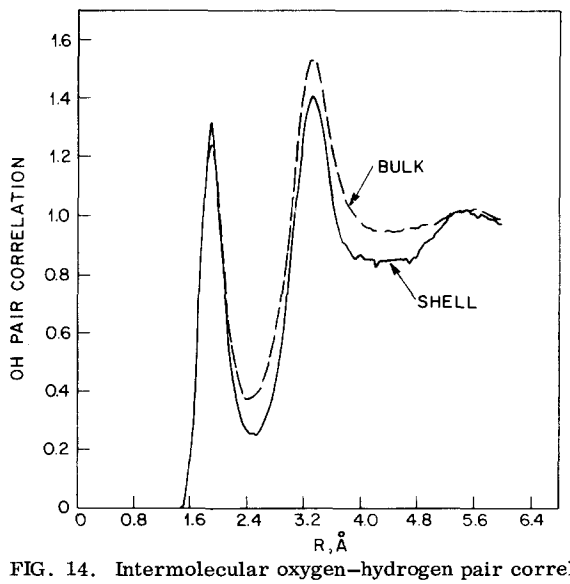

FIG. 14. Intermolecular oxygen–hydrogen pair correlation functions $g_{\mathrm{OH}}(r)$ monitoring the structure-promoting influence of the LJ particles. All water pairs comprising at least one hydration shell member contribute to the shell average. All other pairs establish the bulk average. The shell function shows more structure than the bulk function.

V. ENERGY CALCULATIONS

A. Energy fluctuations and heat capacity

The total energy of the 216 particle system was preset to -105.7ϵ per particle, i.e., -8.01 kcal/mole (the experimental value for pure water at our run temperature of 305.5 °K is -7.99 kcal/mole).[25,26]

In analyzing the potential energy of the shell molecules and the rest, which will be called the bulk molecules, we shall proceed as follows: Let V_j represent that part of the total interaction energy of the system which is contributed by molecule j:

$$V_j = \frac{1}{2}\sum_{\substack{k=1\\k\neq j}}^{216} V_{jk} \ .$$

V_{jk} is the interaction energy between particles j and k. We now define U_s, the energy of the shell molecules as

$$U_s = \frac{1}{N_h}\sum_{h}^{N_h} V_h \ ,$$

where h symbolizes a member of the hydration shell molecules. Notice that U_s is defined as an average over all the N_h molecules belonging to the shell.

Simultaneously, for later purposes the bulk interaction energy U_b is defined as

$$U_b = \frac{1}{N_b}\sum_{b}^{N_b} V_b \ ,$$

and of course $N_b = 214 - N_h$. Thus an average interaction energy U_w of all the water molecules N_w can be defined by

$$214\, U_w = N_h U_s + N_b U_b \ .$$

The hydration shell is defined as before [Sec. IV.A] in terms of the neon–water distance. Figure 15 shows the fluctuations in time of the average interaction energy U_s of the shell molecules during the dynamics run. It is interesting to notice the presence of large low-frequency fluctuations in $U_s(t)$. As we shall see, these are consequences of structural fluctuations, which can also be observed in many other dynamic and energetic properties (but not in the time-averaged structural properties discussed so far).

To detect these structural changes, the dynamics run was divided into nine "time slices" (indicated by the vertical lines in Fig. 15) with a length of 3000τ each (except the last one). The time averages were calculated not only for the whole run, but also separately for the different segments. To illustrate the structural fluctuations we will also show time averages over the two composite segments from 3000τ to $12\,000\tau$ and from $12\,000\tau$ to $21\,000\tau$, which are essentially high and low potential energy periods, respectively. It should be mentioned that there is no simple relation between these energetically different states, and the observed two different geometric states of the neon pair (i.e., when the pair is enclosed in one or two adjacent water cages, respectively). In both geometric states low and high potential energy states occur.

These large energy fluctuations can explain the large

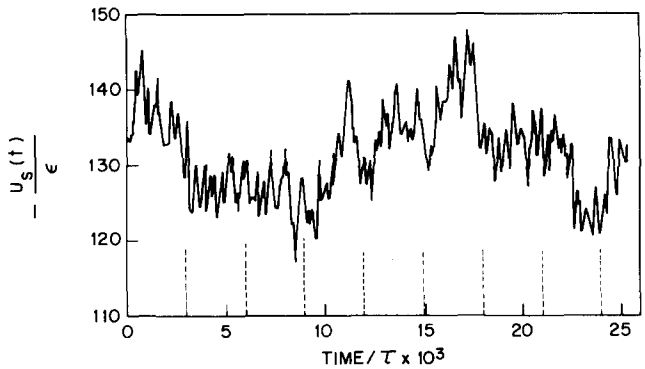

FIG. 15. Fluctuations of the average interaction energy U_s of the hydration shell molecules during the dynamics run (for definition of U_s see text). Vertical broken lines indicate "time slices" used to detect structural fluctuations by averaging over different periods.

partial molar heat capacities of nonpolar solutes in water. To get a *rough* estimate for the heat capacity of the hydration shell water, one can introduce the mean square fluctuations $\langle(\Delta U_s)^2\rangle$ in a formula derived for canonical ensembles and used in Monte Carlo calculations[27]:

$$C_v^i/R = n\langle(\Delta U_s)^2\rangle/k^2T^2 \ .$$

C_v^i is the structural part of the heat capacity at constant volume, for T we use the time averaged temperature of the total system, and for n we take the average number of hydration water molecules used in calculating $\langle(\Delta U_s)^2\rangle$. We find $\langle(\Delta U_s)^2\rangle = 39.5\epsilon^2$ and $n = \langle N_h\rangle = 19.9$, giving

$$C_{v,\,\text{shell}} = C^i_{v,\,\text{shell}} + 6 = 28.1 \text{ cal/deg mole} \ .$$

Interpolating from Rahman and Stillinger's results[2] we get for pure ST2-water at the same temperature:

$$C_{v,\,\text{pure}} = 23.2 \text{ cal/deg mole} \ .$$

So finally we can estimate an excess heat capacity of the hydration shell molecules

$$\Delta C_v = C_{v,\,\text{shell}} - C_{v,\,\text{pure}}$$
$$= 28.1 - 23.2 = 4.9 \text{ cal/deg mole}$$

and if we assume about 14 hydration water molecules, we end up with a roughly estimated excess per mole solute of

$$\Delta C_v = 68.6 \text{ cal/deg mole} \ ,$$

comparable to the experimental values of 30 to 65 cal/deg mole for the partial molar heat capacity of noble gases in water.[6,28] We also monitored the average intrashell interaction energy U_i.

$$N_h U_i = \frac{1}{2}\sum_{h}^{N_h}\sum_{\substack{h'\\h\neq h'}}^{N_h} V_{hh'} \ .$$

The summation considers all the interactions within the shell. The mean squared fluctuation of this property was found to be $\langle(\Delta U_i)^2\rangle = 32.3\epsilon^2$ and can be used in exactly the same manner as described above to estimate the heat capacity. Finally this yields an excess value of

$$\Delta C_v = 36.9 \text{ cal/deg mole solute} \ ,$$

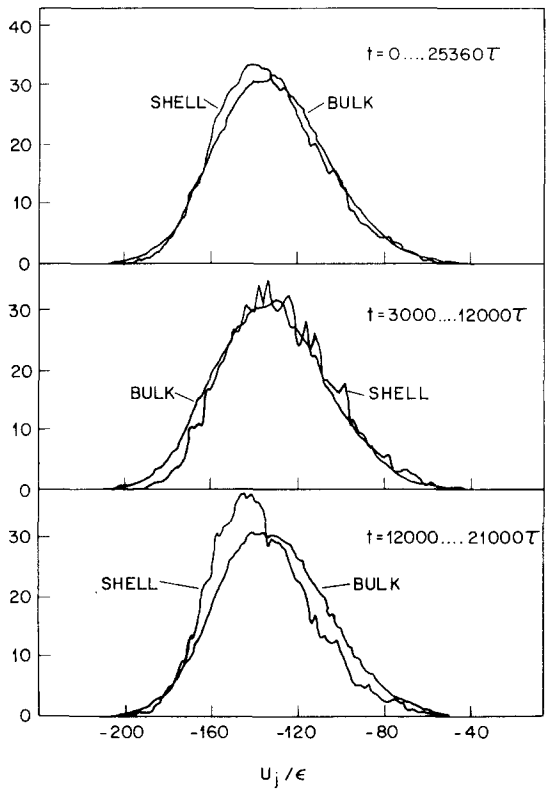

FIG. 16. Distribution functions for interaction energies as defined in Sec. V.A. The curves show occurrence probabilities in units of 10^{-3} for intervals of width $\Delta V = 2.0\epsilon = 0.15$ kcal/mole. (a) Average over the total run, (b) average over high energy period $t = 3000\tau - 12\,000\tau$, (c) average over low energy period $t = 12,000\ \tau - 21,000\tau$.

which is still within the scope of the experimental values and shows the uncertainty of the estimating procedure.

B. Average interaction energy

The previously defined interaction energy U_w of the total water system can also be written as

$$U_w = \frac{1}{N-2}\left\{\frac{1}{2}\sum_{j=1}^{2}\sum_{k=3}^{N} V_{\mathrm{LJ},jk} + \sum_{j=3}^{N-1}\sum_{k=j+1}^{N} V_{jk}\right\} .$$

$V_{\mathrm{LJ},jk}$ is the interaction energy between neon j and water molecule k, V_{jk} is the interaction energy between water molecules j and k. Then the time averages over the total run of U_w and U_s (also defined in Sec. A) are calculated

$$\langle U_w \rangle = -130.756\epsilon = -9.905 \text{ kcal/mole} ,$$

$$\langle U_s \rangle = -131.702\epsilon = -9.976 \text{ kcal/mole} .$$

From these data the corresponding value for the bulk water is obtained (see Sec. A)

$$\langle U_b \rangle = -130.659\epsilon = -9.897 \text{ kcal/mole} .$$

Because only differences are considered, no corrections for the cutoff are added (the corresponding value for pure water, interpolated from Ref. 2 data $\langle U_{\mathrm{pure}} \rangle = -9.97$ kcal/mole cannot be used for comparison, because different cutoffs were used). Thus we get

$$\Delta U = \langle U_s \rangle - \langle U_b \rangle = -1.043\epsilon$$
$$= -79 \text{ cal/mole} .$$

Now, if we assume again that in the low concentration limit we have 14 hydration water molecules per neon, we end up with an energy change per mole solute of

$$\Delta U = -1.1 \text{ kcal/mole solute} ,$$

which is in good agreement with the observed small exothermic enthalpy changes of -1.0 to -2.0 kcal/mole of solute.[5,28]

C. Interaction energy distributions

We shall now consider the manner in which V_h or V_b (which were written down in Sec. A) are distributed over possible values. Using an interval of energy $\Delta V = 2.0\epsilon = 0.15$ kcal/mole we have monitored the frequency of occurrence of various values of V_j and the histograms have been plotted separately for the bulk and for the shell molecules. These are shown in Figs. 16(a)–(c).

The distributions show a single broad bell-shaped curve. The maximum for the shell molecules is higher and shifted slightly to lower energies compared to the bulk molecules (corresponding to more structured water at lower temperatures). There is a correspondence between the U_s (defined in Sec. V.A and displayed in Fig. 15) and the shapes of the distributions shown in Fig. 16(b), (c). During the time when U_s has high values (in Fig. 15 the time from 3000 to 12 000τ) the two distributions are overlapping [Fig. 16(b)] and when it has low values (in Fig. 15 the time from 12 000 to 21 000τ) they are well separated [Fig. 16(c)].

D. Pair interaction energy distributions

In the studies on pure water[1,2] the distribution function for pair interaction energies between two water molecules was calculated. This is repeated here, but separately for bulk and shell water [Fig. 17(a)–(c)]. Bulk and shell having been defined as before, a pair energy V_{jk} is considered in the shell distribution if one or both members j and k belong to the shell molecules, otherwise it is made part of the bulk distribution.

On the negative energy side these distributions show a slightly more pronounced shoulder structure for the shell average (corresponding to "more structured" water). Apart from the region between -20ϵ and $+20\epsilon$ which is mostly populated by distant pairs, the smaller number of shell pair energies compared to the bulk distributions originates from the fact that the neighboring neons exclude other water molecules from close approach.

For different time periods, shell distributions with a less pronounced shoulder structure change to those that show more developed shoulders, corresponding, respectively, to periods with high and low average potential energy of the shell molecules (see Fig. 15).

E. Bond energy distribution

The clathrate and iceberg models of hydrophobic hydration would require an increase of hydrogen bonding

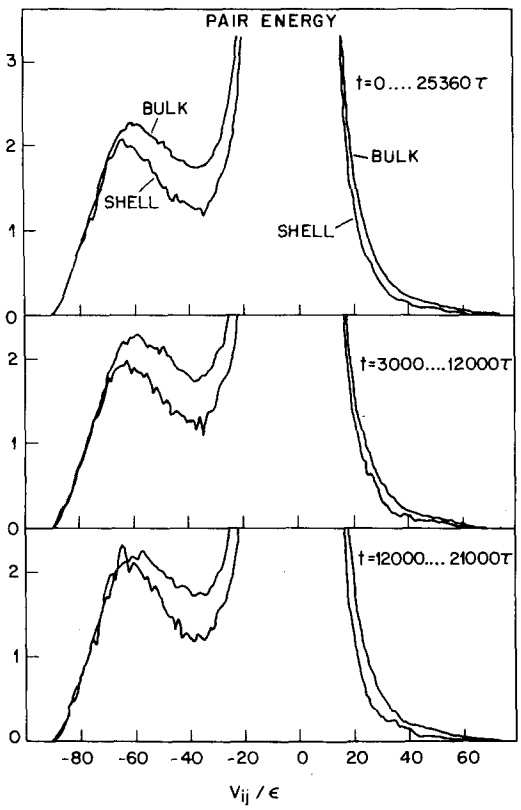

FIG. 17. Distribution functions for pair interaction energies V_{ij}. A pair energy V_{ij} is considered to belong to the shell distribution if one or both members i and j are shell molecules, otherwise it contributes to the bulk distribution. The curves show occurrence probabilities in units of 10^{-3} for intervals $\Delta V = 1.2\epsilon = 0.091$ kcal/mole. (a) Average over the total run, (c) average over high energy period, (c) average over low energy period.

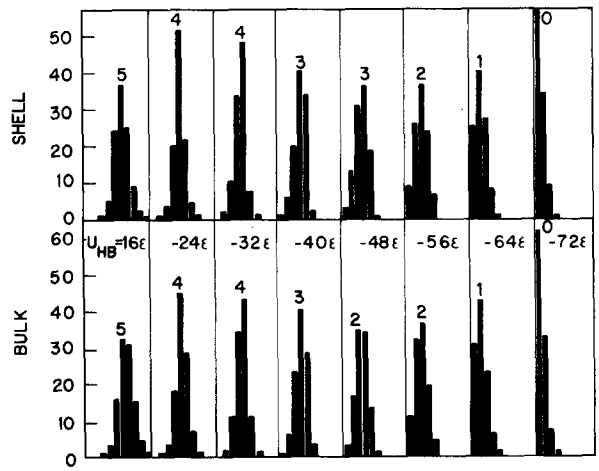

FIG. 18. Distribution of molecules according to the number of hydrogen bonds in which they engage for a series of alternative hydrogen bond strengths U_{HB}. Results for bulk and shell molecules are shown separately.

in the neighborhood of the neons, whereas NMR proton shift measurements mentioned previously seem to contradict this picture. Therefore, the same bond energy distribution calculations as in pure water[1] were carried out. Whenever the interaction energy V_{ij} for a given pair of molecules i and j lies below a negative cutoff value U_{HB} ($V_{ij} < U_{HB}$) we say the pair is hydrogen bonded. Then for each water molecule j the number N_{HB} of "hydrogen bonded" partners is counted. This permits construction of histograms showing the number of water molecules $n(N_{HB})$ that are hydrogen bonded simultaneously to N_{HB} other molecules and finally we get a probability distribution

$$p(N_{HB}) = n(N_{HB}) \Big/ \sum_{N_{HB}=0}^{\infty} n(N_{HB}) \ .$$

This can be done for a series of plausible U_{HB} values. Figure 18 shows $p(N_{HB})$ for

$$U_{HB} = -8\epsilon(i+1) \ , \quad i = 1 \cdots 8 \ ,$$

separately for bulk and shell molecules. No drastic differences between shell and bulk molecules are visible. For each distribution the average number of hydrogen bonds per molecule was calculated by

$$\overline{N_{HB}} = \sum_{N_{HB}=0}^{\infty} N_{HB} \cdot p(N_{HB}) \ ,$$

and is presented in Table II.

For strict choices of U_{HB} (strong interactions) the average number of hydrogen bonds is higher in the shell than in the bulk; but for permissive definitions this behavior is reversed. This is because the shell molecules do not have as many water neighbors for attractive interaction. With a realistic choice of U_{HB} (isotope fractionation results[29] suggest $U_{HB} \simeq -3.2$ kcal/mole) we find a slight increase of hydrogen bonding in the hydration shell, smaller than expected by the previously mentioned models. Rigorously one should compare the hydration shell properties with those of pure water, because the geometrically defined bulk is also slightly influenced by the presence of the solute. But as other fea-

TABLE II. Average number of hydrogen bonds per water molecule $\overline{N}_{HB}$ in bulk and shell, calculated for different hydrogen bond energy definitions U_{HB}. The last row shows the relative difference between shell and bulk.

$-U_{HB}$(kcal/mole)	1.212	1.818	2.424	3.03	3.636	4.242	4.848	5.454
$\overline{N}_{HB,shell}$	5.15	4.03	3.50	3.06	2.56	1.93	1.21	0.54
$\overline{N}_{HB,bulk}$	5.54	4.19	3.52	2.98	2.40	1.74	1.05	0.46
$\Delta\overline{N}_{HB}/\overline{N}_{HB,bulk}$	−0.07	−0.04	−0.01	0.03	0.07	0.11	0.15	0.17

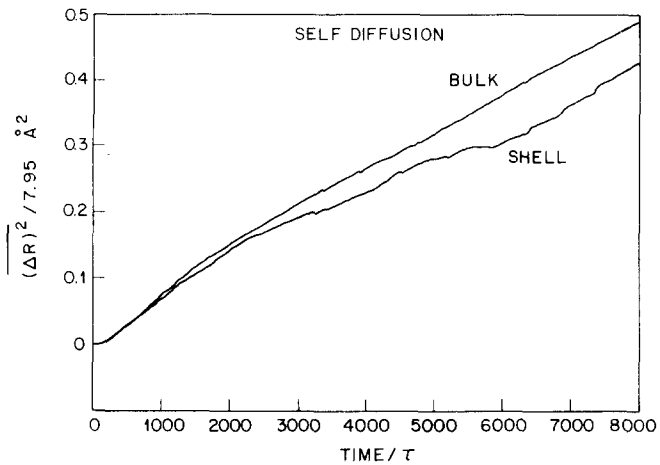

FIG. 19. Mean-square center-of-mass displacements of hydration shell and bulk water molecules. All those water molecules contribute to the shell average that are initially within the first subshell of at least one neon ($d_{\mathrm{Necw}} \leq 3.7$ Å).

tures show (for example dynamical properties), bulk averages obtained in this way are not very different from previously established pure water values.

VI. DYNAMIC PROPERTIES

A. Self-diffusion

The self-diffusion coefficient, strictly speaking, can be determined by the long-time limiting slope of the mean square center-of-mass displacement (Fig. 19):

$$D = \lim_{t\to\infty} \{\langle[\Delta \mathbf{R}_j(t)]^2\rangle/6t\} ,$$

$$\Delta \mathbf{R}_j(t) = \mathbf{R}_j(t_0 + t) - \mathbf{R}_j(t_0) ,$$

$\mathbf{R}_j(t)$ is center of mass coordinate vector of water molecules j at time t. It usually suffices to examine slopes over a finite time interval. $\langle[\Delta \mathbf{R}_j(t)]^2\rangle$ is calculated separately for bulk and shell molecules. To avoid the diffusion of hydration molecules out of the shell during the observation period, only those water molecules are used to calculate the shell average that are within the *first* subshell of at least one neon at time $t = t_0$:

$$d_{\mathrm{NecW}}(t_0) = |\mathbf{R}_{\mathrm{Ne}}(t_0) - \mathbf{R}_{\mathrm{cW}}(t_0)| \leq 3.7 \text{ Å} .$$

All other molecules contribute to the bulk average. The same distinction between bulk and shell is used for all dynamic properties. Again separate averages for the low and high potential energy states are formed. The results are presented in Table III.

These results show that water molecule self-diffusion is slower in the hydration shell by about 20%. This is comparable to values estimated from NMR diffusion studies of aqueous solutions of nonelectrolytes.[16,17]

In monitoring the difference in self-diffusion between shell and bulk we have noticed a correlation between the high energy and low energy periods (see Fig. 15); during the former the shell and the bulk properties are almost identical and during the latter they are distinctly different. Figure 19 of course shows the overall average behavior.

The interpolated experimental value of the diffusion coefficient of pure water[30] ($D_{32.3\,^\circ\mathrm{C}} = 2.74 \cdot 10^{-5}$ cm^2/sec) is about 20% smaller than the bulk value shown in Table III; the same discrepancy was observed in prior pure water simulation. This shows that the influence of the hydration shell on the bulk average is not very strong.

TABLE III. Self-diffusion coefficients for bulk and shell water molecules in units of 10^{-5} cm^2/sec. The time intervals for the respective evaluations are indicated.

	Total run 0–25 360τ	High-energy period 3000–12 000τ	Low-energy period 12 000–21 000τ
$D_{\mathrm{bulk\ water}}$	3.46	3.48	3.47
$D_{\mathrm{shell\ water}}$	2.91	3.20	2.74
D_s/D_b	0.84	0.92	0.79

B. Relative diffusion

To get information about the cooperative nature of translational motions in the hydration shell, the mean squares of the relative displacements of originally neighboring molecules were calculated

$$\langle(\Delta \mathbf{R}(t))^2\rangle \equiv \langle(\mathbf{R}_{jk}(t_0) - \mathbf{R}_{jk}(t_0 + t))^2\rangle ,$$

$$\mathbf{R}_{jk}(t) = \mathbf{R}_j(t) - \mathbf{R}_k(t) ,$$

where $\mathbf{R}_j(t)$ is the center-of-mass coordinate of molecule j. Only those pairs of water molecules j and k are considered which have a center-of-mass distance $d_{jk} \leq 3.7$ Å at time $t = t_0$. From the limiting slope of $\langle[\Delta \mathbf{R}(t)]^2\rangle$ relative diffusion coefficients can be calculated (Fig. 20).

Table IV shows the relative coefficients $D_{mm'}$, together with 2 D_{self}, the value one would have obtained in the case of totally uncorrelated motions. Note that in this case shell and bulk are again distinguished by a neon–water distance of $d \leq 3.7$ Å. We find augmented dynamical correlation in translational motion in the hydration shell compared to the bulk. It needs to be mentioned that this augmented dynamical correlation at short times will eventually (i.e., in the limit of infinite time) dis-

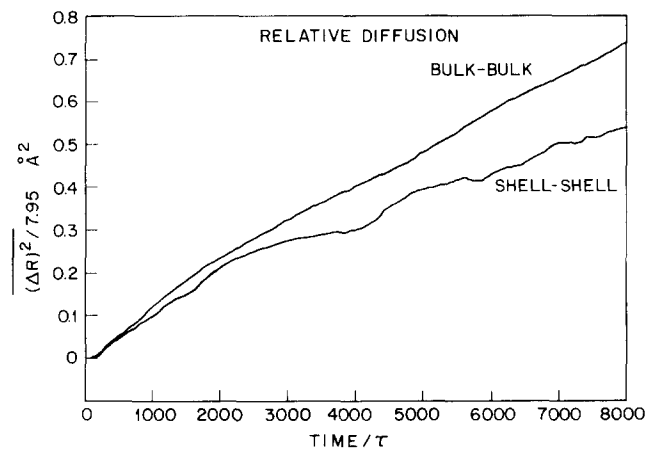

FIG. 20. Relative diffusion of pairs of molecules. The definition of bulk and shell is as in Fig. 19. The relevant quantities are specified in the text (Sec. VI.B).

TABLE IV. Relative diffusion coefficients for bulk and shell water molecules in units of 10^{-5} cm^2/sec.

	$D_{mm'}$	$2D_{self}$	$D_{mm'}/(2D_{self})$
Bulk–bulk	5.17	6.92	0.75
Shell–shell	3.34	5.82	0.57
D_{shell}/D_{bulk}	0.65	0.84	

appear. However for intermolecular NMR relaxation the function we have considered is of considerable significance and hence during this time the pair diffusion cannot be thought of as uncorrelated motion of its members.

C. Reorientational motion

The altered reorientational behavior of the water molecules in the hydration shell has been investigated by nuclear magnetic relaxation methods[31] as well as by dielectric relaxation measurements.[32] Both methods probe the decay of autocorrelation functions Γ_l for Legendre polynomials $P_l(\cos\phi)$ for various molecule-fixed unit vectors $\hat{\mu}_j$:

$$\Gamma_l(t) = \langle P_l(\hat{\mu}_j(t_0) \cdot \hat{\mu}_j(t_0 + t)) \rangle \ .$$

Dielectric relaxation is determined by Γ_1. The nuclear magnetic relaxation of the water protons provides information about the decay of Γ_2 of the proton–proton vector in the water molecule (parallel to the y axis, $\hat{\mu}_y$).

Γ_1 and Γ_2 for all three molecular axes were determined. (See Figs. 21 and 22 for two typical examples of the 6 possible functions. Relevant information about all the correlation functions is given in Table V). An initial period of libration (less than 0.1 psec) is followed by a roughly exponential decay. Table V contains the correlation times τ_1 and τ_2 obtained by fitting an exponential to the autocorrelation functions, neglecting the first part. The shell average is formed by all molecules within a distance of $d_{Ne\,c\,w} \leq 3.7$ Å of at least one neon at time $t = t_0$.

Table V reveals the following remarkable facts:

(1) The ratios τ_1/τ_2 are between 1.5 and 2.6. This indicates a deviation from pure Brownian rotational diffusion, for which $\tau_1/\tau_2 = 3$ is expected. The z-axis reorientation is closest to diffusional motion, whereas the y-axis motion (determining NMR relaxation) shows strong deviations.

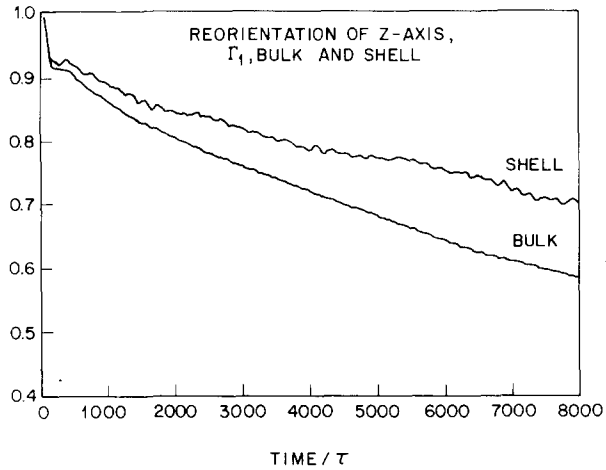

FIG. 21. Reorientation correlation functions (using first-order Legendre polynomials) for dipole directions of shell and bulk water molecules.

(2) The shell correlation times are increased by a factor of 1.2 to 1.7 compared to the bulk. These increases are strongest for z-axis motion.

The agreement with experimental values is good. Using the temperature dependence of Krynicki's[34] proton magnetic relaxation time measurements of pure water and the value $\tau_2 = 2.5$ psec[33] for the y-axis reorientation at 25 °C, we get an experimental value $\tau_{2,y} = 2.1$ psec for 32.2 °C. This is equal to the bulk value in Table V. Also the increase of about 20% in passing from the bulk to the hydration shell is within the range of the experimentally found factors of 1.1–2.0 for different nonelectrolyte solutes.[16,17]

If τ_1 of z-axis reorientation has to be multiplied by factors 1.5 to 2.0[35,36] to be comparable with dielectric relaxation times, it follows that 5.7 psec $\leq \tau_{D,\,bulk} \leq 7.6$ psec. This value can be compared with the dielectric relaxation time of pure water at 32.3 °C,[37] namely $\tau = 6.8$ psec. Pottel and Kaatze[18] measured dipolar relaxation-time enhancement factors for nonpolar solutes of 1.5 to 2.8. They observed a dependence upon molar volume ratio between solute and solvent, so that it is quite reasonable that our value of 1.7 should be located in the lower part of the specified range.

VII. CONCLUSIONS

The present results support the models of hydrophobic hydration deduced from thermodynamic and spectroscopic experimental findings. Inert particles are sur-

TABLE V. Molecular reorientation correlation times for the three principal axes of the water molecules in units of 10^{-12} sec.

	z axes			y axes			x axes		
	Bulk	Shell	τ_{shell}/τ_{bulk}	Bulk	Shell	τ_{shell}/τ_{bulk}	Bulk	Shell	τ_{shell}/τ_{bulk}
τ_1	3.82	6.59	1.73	3.42	4.03	1.18	2.87	3.73	1.30
τ_2	1.61	2.55	1.58	2.12	2.65	1.25	1.66	2.02	1.22
τ_1/τ_2	2.37	2.58		1.61	1.52		1.73	1.85	

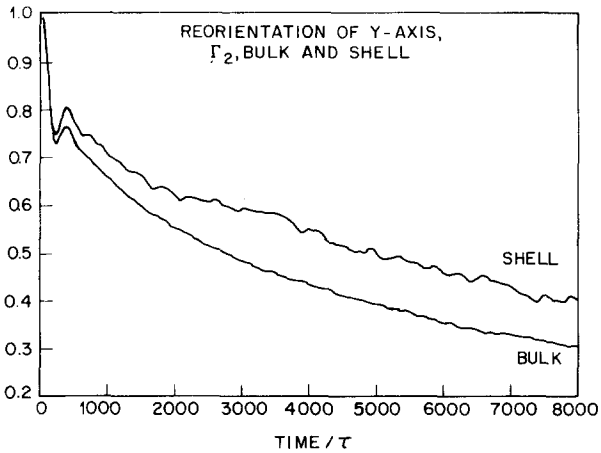

FIG. 22. Reorientation correlation functions of the water molecule y axes (using second-order Legendre polynomials) for shell and bulk water molecules.

rounded by water cages, whose orientational structure can be compared with clathrates. But the observed structure promotion does not lead to an immobilization of the hydration water as it does in solid structures; only a small reduction of mobility is seen to occur.

Although a system of two neons was observed during a very long time-period (from the computational point of view!), statistics are by far insufficient to allow definite conclusions about hydrophobic interaction or hydrophobic association. Nevertheless the behavior of the neon pair in this run, as well as in the previous one[3] suggests the existence of solvent-separated hydrophobic association. In both cases the originally close, neighboring neons did separate after some time and were subsequently trapped in two adjacent water cages up to the end of the simulation run. The orientation of the molecules in the intermediate water layer indicates that the two cages are linked together by these common members, as proposed by Clark *et al.*[22]

To get a more precise answer to these questions, a special simulation run would be necessary. By fixing the neon pair distance at different values it should be possible to determine the average force acting between the two neons, or equivalently to determine the solvation free energy of the systems as a function of the distance. This was tried by Dashevsky and Sarkisov[4] with MC calculations, but their method to calculate the free energy is subject to large statistical errors.

We believe that the calculations reported here can be valuable in designing a subsequent study of hydrophobic interaction in which statistical accuracy is improved.

ACKNOWLEDGMENT

One of the authors (A.G.) is grateful for financial support by the Deutsche Forschungsgemeinschaft.

[1]A. Rahman and F. H. Stillinger, J. Chem. Phys. **55**, 3336 (1971).
[2]F. H. Stillinger and A. Rahman, J. Chem. Phys. **60**, 1545 (1974).
[3]A. Rahman, in Report of Workshop on "Ionic Liquids," Centre Européen de Calcul Atomique et Moléculaire, Orsay, France, 1974, p. 263.
[4]V. G. Dashevsky and G. N. Sarkisov, Mole. Phys. **27**, 1271 (1974).
[5]W. Kauzmann, Adv. Protein Chem. **14**, 1 (1959).
[6]F. Franks, *Water—A Comprehensive Treatise*, edited by F. Franks (Plenum, New York, 1973), Vol. 2, Chap. 1.
[7]F. Franks, in Ref. 6, (Plenum, New York, 1975), Vol. 4, Chap. 1.
[8]A. Ben-Naim, *Water and Aqueous Solutions* (Plenum, New York, 1974).
[9]H. S. Frank and M. W. Evans, J. Chem. Phys. **13**, 507 (1945).
[10]G. Némethy and H. A. Scheraga, J. Chem. Phys. **36**, 3401 (1962).
[11]H. G. Hertz, Ber. Bunsenges. Phys. Chem. **68**, 907 (1964).
[12]D. N. Glew, J. Phys. Chem. **66**, 605 (1962).
[13]H. G. Gertz, and W. Spalthoff, Z. Elektrochem. Ber. Bunsenges. Phys. Chem. **63**, 1096 (1959); J. Clifford, B. A. Pethica, Trans. Faraday Soc. **61**, 182 (1965).
[14]W. Y. Wen, H. G. Hertz, J. Solution Chem. **1**, 17 (1972); M. C. R. Symons, J. Phys. Chem. **71**, 172 (1967).
[15]D. N. Glew, H. D. Mak, and N. S. Rath, Chem. Commun. **1968**, 264; in *Hydrogen-Bonded Solvent Systems*, edited by A. K. Covington and P. Jones, (Taylor and Francis, London, 1968), pp. 197–210.
[16]E. V. Goldammer, H. G. Hertz, J. Phys. Chem. **74**, 3734 (1970).
[17]E. V. Goldammer and M. D. Zeidler, Ber. Bunsenges. Phys. Chem. **73**, 4 (1969); H. G. Hertz and M. D. Zeidler, *ibid.* **68**, 821 (1964).
[18]R. Pottel and U. Kaatze, Ber. Bunsenges. Phys. Chem. **73**, 437 (1969).
[19]H. G. Hertz and C. Rädle, Ber. Bunsenges. Phys. Chem. **77**, 521 (1973).
[20]H. G. Hertz and W. Y. Wen, Z. Phys. Chem. Frankfurt **93**, 313 (1974).
[21]G. Jaccuci and A. Rahman, Report on workshop on "Long-Time-Scale Events," Centre Européen de Calcul Atomique et Moléculaire, Orsay, France, 1974, p. 32.
[22]A. H. Clark, F. Franks, M. D. Pedley, and D. S. Reid, Faraday Trans. I **73**, 290 (1977).
[23]A. Rahman, Phys. Rev. A **136**, 405 (1964).
[24]F. H. Stillinger, J. Solution Chem. **2**, 141 (1973).
[25]N. E. Dorsey, *Properties of Ordinary Water Substance* (Reinhold, New York, 1940).
[26]D. Eisenberg and W. Kauzmann, *The Structure and Properties of Water* (Oxford University, New York, 1969).
[27]J. L. Lebowitz, J. K. Percus, and L. Verlet, Phys. Rev. **153**, 250 (1967).
[28]B. B. Benson and D. Krause, Jr., J. Chem. Phys. **64**, 689 (1976).
[29]W. T. King and R. E. Barletta, J. Chem. Phys. **67**, 180 (1977).
[30]R. Mills, J. Phys. Chem. **77**, 685 (1973).
[31]M. D. Zeidler in *Water—A Comprehensive Treatise*, edited by F. Franks (Plenum, New York, 1973), Vol. 2, Chap. 10.
[32]J. B. Hasted, in Ref. 31, Vol. 2, Chap. 7.
[33]H. G. Hertz, in Ref. 31, Vol. 3, Chap. 7.
[34]K. Krynicki, Physica (Utrecht) **32**, 167 (1966).
[35]J. G. Powles, J. Chem. Phys. **21**, 633 (1953).
[36]T. W. Nee and R. W. Zwanzig, J. Chem. Phys. **52**, 6353 (1970).
[37]J. B. Hasted, in *Water—A Comprehensive Treatise*, edited by F. Franks (Plenum, New York, 1972), Vol. 1, Chap. 7.